A BOWED STRING PHYSICAL MODEL INCLUDING FINITE-WIDTH THERMAL FRICTION AND HAIR DYNAMICS

Esteban Maestre
CCRMA – Stanford University
esteban@ccrma.stanford.edu

Carlos Spa
Universidad Federico Santa María
carlos.spa@usm.cl

Julius O. Smith III
CCRMA – Stanford University
jos@ccrma.stanford.edu

ABSTRACT

In light of the promising results obtained by driving a low-complexity digital waveguide (DW) violin model with synthetic bowing gestures [1], we currently explore the possibilities of combining DW and finite-difference time-domain (FDTD) frameworks to construct refined, yet efficient physical models of string quartet instruments. We extend previous approaches by combining a finite-width bow-string interaction model with a dynamic friction model based on simulating heat diffusion along the width of the bow. Bow hair dynamics are incorporated in the bow-string interaction, which includes two transversal string polarizations. The bridge termination is realized using an efficient, passive digital reflectance matrix obtained from fitting admittance measurements. In this paper we present and discuss the current status and future directions of our modeling work.

1. INTRODUCTION

Bowed strings can be considered as one of the key challenges in computer-generated instrumental sound. In an attempt to provide means to generate realistic synthetic bowed-string performances by computer, for a number of years we have been interested in measuring, modeling, and synthesizing bowing gestures [1]. Be it via sample-based techniques incorporating spectral-domain sound transformation, or via physical modeling synthesis, the use of synthetic bowing gestures to drive violin sound generation has proved to dramatically enhance the realism of generated performances [1] [2]. In consideration of the promising results recently obtained by driving a simplified digital waveguide physical model [3] with rendered bow strokes, we are interested in constructing refined bowed-string models that can serve as a basis for further developing bowing synthesis.

Today, the physics of bowed strings has been studied for over 150 years. Since Helmholtz [4] described the ideal bowed-string motion in 1862, many scientists have pursued research towards understanding and modeling the sound production mechanisms behind such expressive instruments. Here we will provide a very brief review. As early as 1914,

---

[1] http://ccrma.stanford.edu/~esteban/bowed/demo14.wav (digital waveguide model)

Raman [5] proposed the first algorithm for bowed-string motion, modeling friction force as a nonlinear function of sliding velocity. Without a computer, he was able to predict most string vibration regimes nowadays understood. Later, Friedlander [6] and Keller [7] simulated Raman's model in a computer, proposing a graphical solution to the friction nonlinearity. A next important step was performed by McIntyre and Woodhouse [8], who further developed Friedlander solution, adding a hysteresis rule for solving the nonlinearity. Then, real-time simulation was made possible by Smith [9, 10], who reformulated bow-string interaction as a scattering junction having a precomputed (noniterative) nonlinear reflection coefficient, and developed efficient techniques to simulate instrument bodies as efficient IIR digital filters. A monumental work by Pitteroff and Woodhouse [11] introduced a finite-width bow-string interaction model including hair dynamics, demonstrating partial slips for the first time. Later, a first dynamic friction model based on simulating the bow-string contact temperature was introduced in [12] and later applied in [13] to a point-bow model, providing simulations that qualitatively matched the hysteretic behavior of friction as observed experimentally through dynamic measurements. For an excellent review of models up to 2004, please refer to [14]. Since then, the introduction of vertical string polarization (perpendicular to the bow direction) into a point-bow model with static friction [15] can be considered a further relevant contribution.

In this paper, we report on our own progress towards a further refinement of current bowed-string simulation approaches. We introduce a model combining a finite-width bow-string interaction model with a dynamic friction model based on simulating heat diffusion along the width of the bow. Bow hair dynamics are incorporated in the bow-string interaction, which includes two transversal string polarizations. The strings are coupled at a bridge termination, which is realized via an efficient, passive digital reflectance matrix obtained from fitting admittance measurements. The rest of the paper is structured as follows. In Section 2 we provide an overview of our framework. Section 3 describes our approach to temperature-dependent friction, while Section 4 introduces bow-string interaction. In Section 5 we describe our model for the bridge admittance. Section 6 presents some preliminary results using our model, and we finally conclude by providing an outlook to further developments.

2. OVERVIEW OF THE MODEL

We develop a bowed-string synthesis framework that combines temperature-driven dynamic friction and finite-width
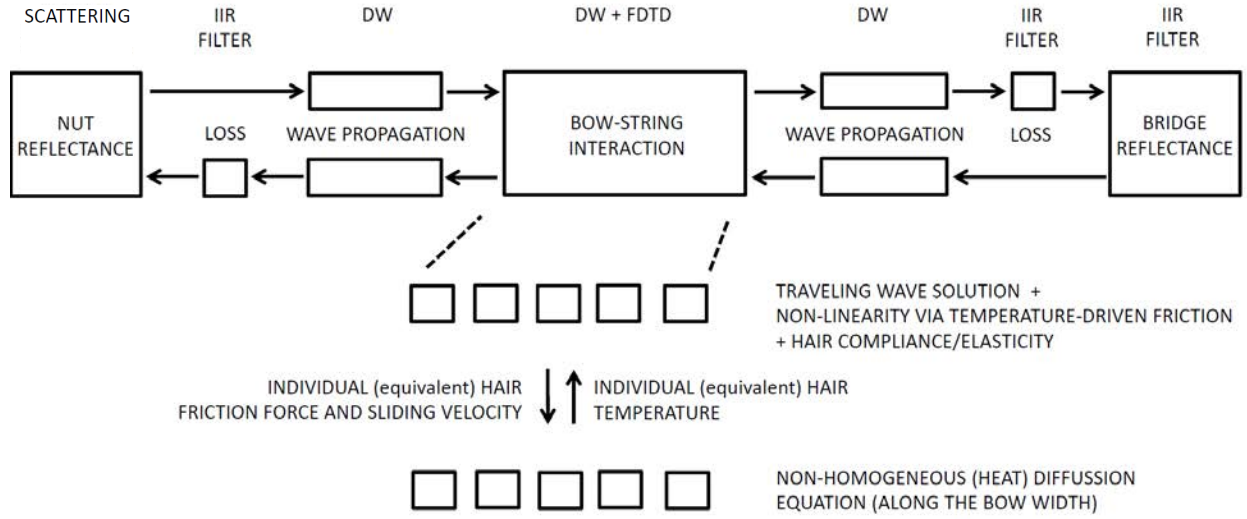
Figure 1: Overview of our model, combining digital waveguide and finite-difference approximations.

bow-string interaction. A schematic illustration is provided in Figure 1. Our framework considers two polarizations of string transverse waves: horizontal (parallel to the bowing direction) and vertical (perpendicular to the bowing direction). The DW framework is used for propagation. Traveling losses in both polarizations are represented as cascaded IIR filters at the end of each direction of the DW.

Horizontal and vertical transverse waves get coupled at the nut, at the bridge, and at the the finite-width bow-string contact. At the nut, both polarizations of all four strings get coupled through a lumped 2×2 admittance matrix with real entries, leading to a reflectance. At the bridge, both polarizations of all four strings get coupled through a lumped 2×2 admittance matrix that represents the instrument body, and contains complex, frequency-dependent elements. The corresponding bridge reflectance matrix is realized via two IIR digital filters, each in parallel form and representing one polarization, as detailed in Section 5.

In an equivalent manner as introduced in [11], bow-string interaction is represented by a line of nodes, each modeling an equivalent hair-string contact. Here, bow and string interact in both polarizations: nonlinear interaction happens on the horizontal plane, while linear interaction happens on the vertical plane. Horizontal-vertical coupling happens through the (vertical) normal force exerted by the string on the hair. In between nodes, we use the traveling wave solution provided by DW. Interaction in the horizontal plane takes place through a nonlinear friction characteristic that is solved at each node. The coefficient of friction is dynamically modulated by temperature changes happening along the nodes in the bow-string contact. Hair compliance and elasticity are included in each node via FDTD, leading to a nonlinearity that can be solved graphically a la Friedlander. In the vertical plane, each node is represented as a lumped junction each with a series-loaded admittance in the form of a mass-loaded parallel spring-dashpot. Details of bow-string interaction are given in Section 4.

Excess temperature along the width of the string-bow

contact is modeled via a non-homogeneous diffusion expression, with two additional terms (see Section 3). Our aim here is to propose a model of dynamic friction which, by providing a hysteric behavior that is qualitatively comparable to that demonstrated by in [12] or in [16], enables finite-width, multi-hair simulation, and is efficient and flexible enough to serve as a platform for investigation on sound synthesis. Temperature is increased via the conduction of heat due to the sliding friction happening at any of the nodes along the bow width, with the source term of the diffusion expression fed by sliding velocity and normal force. Temperature loss is caused either by convection during sliding, or by diffusion.

For the moment, we are ignoring the effect of torsional string vibration or the body of the bow. Moreover, we acknowledge that the individual equivalent hairs are represented as independent mechanical systems, ignoring any hair-hair interaction.

3. THERMAL FRICTION

Temperature of the string section in contact with the bow hairs is simulated by spatio-temporal discretization of the one-dimensional, non-homogeneous diffusion relation in Eq. (1), where $T(x, t)$ represents the relative temperature (with respect to ambient temperature) at position x along the string at time t, α is the diffusivity, v_Δ^x is the equivalent hair-string differential (sliding) transversal velocity, and F_s^x is the equivalent hair-string friction force. Inspired by the convolution integral approach introduced in [12], we re-formulate the problem to enable one-dimensional heat diffusion and to avoid expensive convolutions. The first two terms of Eq. (1) correspond to the homogeneous diffusion, while the third and fourth respectively correspond to losses by convection with the rosin, and temperature increase (conduction) by friction. Parameters C_C and C_H can be computed as a function of a specific heat capacity governing heat transfer at the hair-string interface. Param-
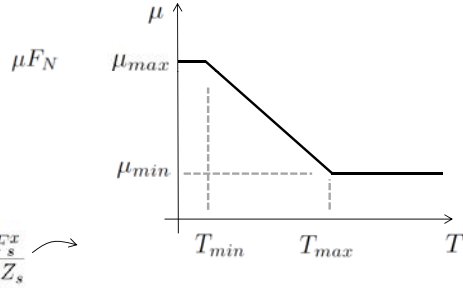
Figure 2: Friction dependence on temperature. Simplifi
piece-wise linear approximation.

Figure 3: Nonlinear bow-string interaction: graphical solution a la Friedlander, accounting for hair elasticity and compliance.

eter C_C modulates temperature loss by convection, while parameter C_H modulates temperature increase by friction.

$$\frac{\partial T(x,t)}{\partial t} - \alpha \frac{\partial^2 T(x,t)}{\partial x^2} + C_C T(x,t)|v_\Delta^x(x,t)| = C_H |F_s^x(x,t)v_\Delta^x(x,t)| \tag{1}$$

Each of the equivalent hair-string segments under simulation is either sticking or slipping. During the sticking phase, the differential velocity v_Δ^x remains zero, and Eq. (1) becomes the relation of homogeneous diffusion, enabling the representation of heat diffusion along the string segment. During the slipping phase, the non-zero value of v_Δ^x brings in the contribution of the other two terms, leading to a temperature increase moderated by convection.

When discretizing partial derivatives for simulation, a forward difference scheme was used for approximating time derivatives, while a centered difference was chosen for approximating space derivatives. Stability analysis of the resulting update equation leads to the requirement in Eq. (2). Given that spatial discretization Δx is imposed by the number of equivalent bow hair-string segments used for simulation of the bow-string interaction (see Section 4), the stability requirement imposes a maximum temporal discretization Δt_{max} for a given diffusivity α.

$$\alpha \frac{\Delta t}{\Delta x^2} < \frac{1}{2} \tag{2}$$

For a given bow width and spatial discretization, the total number of nodes used for simulation of Eq. (1) will result from also accounting for the length of the string segment for which heat diffusion is computed beyond the bow. At the boundaries of such segments, relative temperature is imposed to be zero. For the nodes corresponding to the width of the bow, string sliding velocity and force (see Section 4) are collected each time step and used in terms three and four of Eq. (1).

The coefficient of friction μ governing hair-string interaction is modeled in terms of a simple relation with temperature at each equivalent hair-string segment (see Figure 2), following the qualitative nature of the experimental results introduced in [12] and applied in [13].
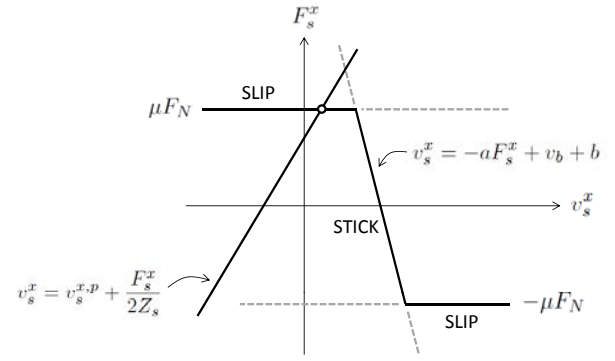
4. BOW-STRING INTERACTION

4.1 Horizontal plane

For each node, hair-string interaction in the horizontal plane (polarization parallel to the bowing direction) is tackled via (i) using a finite-difference approximation to simulate hair dynamics, and (ii) graphically solving the nonlinear friction problem by means of a modified Friedlander construction [6] that accounts for hair dynamics in a straightforward manner. In between nodes, we rely on the traveling wave solution provided by DW. For each node (i.e., equivalent hair) in the bow-string segment, let us define: v_s^x as the transverse horizontal string velocity; $v_s^{x,p}$ as the the transverse horizontal string velocity as computed by only taking into account the incoming waves arriving from adjacent nodes via DW; v_h^x as the longitudinal velocity of the equivalent hair as relative to longitudinal bow velocity v_b; v_Δ^x as the hair-string differential velocity; F_s^x as the string transverse horizontal (friction) force; and Z_s as the string transverse impedance. At all times, the string motion obeys

$$v_s^x = v_s^{x,p} + \frac{F_s^x}{2Z_s}, \tag{3}$$

with

$$\begin{aligned} |F_s^x| &< \mu F_N & \text{(STICK)}, \\ F_s^x &= \text{sign}(v_\Delta^x)\mu F_N & \text{(SLIP)}, \end{aligned} \tag{4}$$

where μ is the temperature-dependent friction coefficient, and F_N is the normal force exerted by the equivalent string segment on the equivalent hair. Moreover, defining $v_\Delta^x = v_s^x - (v_b + v_h^x)$ we have

$$v_s^x = v_b + v_h^x \qquad \text{(STICK)}. \tag{5}$$

Now, in order to express v_s^x in Eq. (5) in terms of F_s^x, we model the dynamics of v_h^x via a massless (parallel) spring-dashpot [11]. The differential equation governing such a system can be written as

$$F_s^x(t) = -k_h \int v_h^x(t)dt - c_h v_h^x(t), \tag{6}$$

where k_h and c_h respectively correspond to the equivalent hair elasticity and compliance constants. By trapezoidal
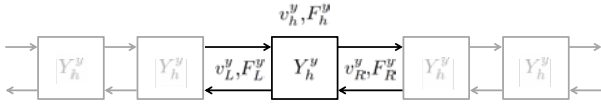
Vertical direction

Figure 4: Vertical admittance of the bow as seen from the string (vertical polarization). Each junction represents one equivalent hair-string segment.

approximation of the integral term, we arrive at

$$v_h^x = -aF_s^x + b, \qquad (7)$$

where a is a positive constant and b depends on previous values of F_s^x and v_h^x. Finally, combining Eq. (5) and (7) we have

$$v_s^x = -aF_s^x + v_b + b \qquad \textsf{(STICK)}, \qquad (8)$$

which, combined with Equations (3) and (4), forms a system of equations which can be solved graphically a la Friedlander [6] by extending the solution proposed in [13] via incorporating hair dynamics in a straightforward manner. This is illustrated in Figure 3.

4.2 Vertical plane

For the polarization that is perpendicular to the bowing direction, each equivalent hair-string segment is treated as a lumped junction between adjacent DW segments. A finite-difference approximation is used to simulate the transversal vertical admittance of the hair as seen from the string. At each junction, the normal force F_N exerted by the string on the hair must equal the total force F_s^y applied by the hair on the string. In our model, we impose that

$$F_s^y = F_b + F_h^y, \qquad (9)$$

where F_b is the vertical force applied by the player, and F_h^y is the vertical force at the junction due to interaction between incoming traveling waves and the junction vertical admittance Y_h^y as seen from each of the two series-connected string segments. Therefore, at each junction (see Figure 4), the string segment vertical velocities v_L^y and v_R^y must both equal the hair vertical velocity v_h^y, while the sum of vertical forces F_L^y and F_R^y applied by the string segments must equal the force F_h^y of the load:

$$\begin{aligned} v_L^y &= v_R^y = v_h^y \\ F_L^y + F_R^y &= F_h^y \end{aligned} \qquad (10)$$

We simulate Y_h^y as a two-pole digital resonator as resulting from constructing an equivalent mass-loaded parallel spring-dashpot structure and discretizing through the trapezoidal approximation. Values for the mass, spring and dashpot can be made dependent on the external vertical force F_b.

5. BRIDGE INPUT ADMITTANCE

In order to allow for both horizontal and vertical polarizations of the transverse waves on the string, we simulate the two-dimensional, driving-point bridge admittance matrix $\mathbf{Y}$
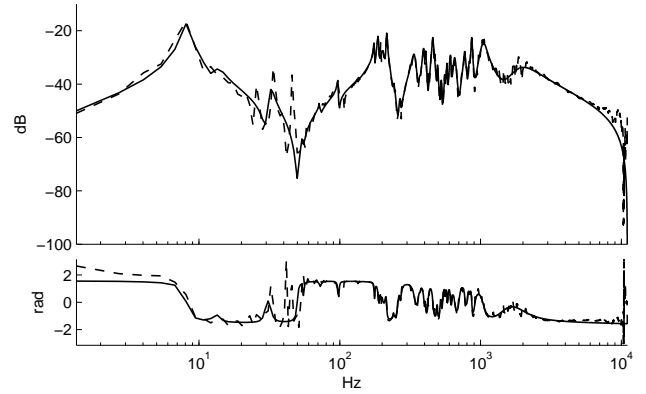

Figure 5: Synthetic admittance $\hat{Y}_{hh}$ modeling example. Magnitude (top) and phase (bottom). Dashed curves: admittance measurement; solid curves: model with $M = 15$.

via the modal framework, by means of an IIR digital filter in parallel form. Starting from the structurally passive admittance matrix formulation introduced in [17] (see Eq. (11)), we developed a technique for fitting the parameters of a passive IIR digital filter to vibration measurements obtained experimentally.

A useful set of structurally passive two-dimensional driving-point admittance matrices can be expressed in the z-domain [17] as

$$\hat{\mathbf{Y}}(z) = \left[\begin{array}{cc} \hat{Y}_{hh}(z) & \hat{Y}_{hv}(z) \\ \hat{Y}_{hv}(z) & \hat{Y}_{vv}(z) \end{array} \right] = \sum_{m=1}^{M} H_m(z)\,\mathbf{R}_m, \quad (11)$$

where each $\mathbf{R}_m$ is a 2×2 positive semidefinite matrix, and each m-th scalar modal response

$$H_m(z) = \frac{1 - z^{-2}}{(1 - p_m z^{-1})(1 - p_m^* z^{-1})}$$

is a second-order resonator determined by a pair of complex conjugate poles p_m and p_m^*. The numerator $1 - z^{-2}$ is the bilinear-transform image of s-plane zeros at DC and infinity, respectively, arising under the "proportional damping" assumption [17]. It can be checked that $H_m(z)$ is positive real for all $|p_m| < 1$ (stable poles). We estimate p_m in terms of the natural frequency and the *half-power* bandwidth of the m-th resonator [18].

Departing from admittance measurements in digital form and the M-th order modal decomposition described in Eq. (11), the problem is posed as a constrained minimization over M mode frequencies, M bandwidths, and M positive semidefinite 2×2 gain matrices. In a first stage, mode frequencies and bandwidths are estimated in the frequency domain via sequential quadratic programming. Then, mode amplitudes are estimated via semidefinite programming while enforcing passivity. We obtain accurate, low-order digital admittance matrix models. The frequency response of the horizontal entry $\hat{Y}_{hh}$ of a cello bridge admittance matrix model ($M = 15$) is displayed in Figure 5. Details about this modeling procedure, including both the measurement and the fitting, can be found in [19].
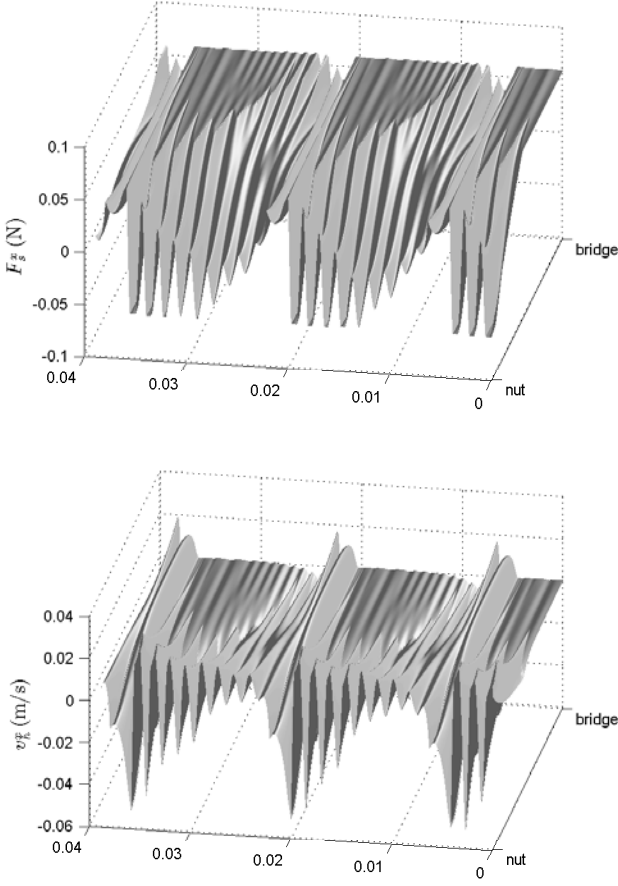
Figure 7: Detail of the spatio-temporal distribution of friction force F_s^x (top) and hair relative horizontal velocity v_h^x (bottom), as seen from the nut side of the bow-string contact. Note that time (bottom axis) is reversed (right to left).

N_B	Δ_x (mm)	f_s (kHz)	Real Time
3	3.3	30.3	4.3%
6	1.6	60.7	9.2%
10	1.0	91.0	18.4%
20	0.5	182.1	49.6%
33	0.3	303.6	119%
60	0.16	546.5	334%

Table 1: Details on computational cost, tested on a 5-year old laptop CPU (Intel P9400). Fully-featured cello simmulation, bowing its C-string with a bow spanning 1 cm, modeled via N_B equivalent hair-string interaction nodes.

Even for moderately fine spatial discretizations, simulations including all four strings and a high-fidelity input bridge admittance can be computed in the vicinity of real-time. Table 1 provides details on computational cost.

In Figure 6 (spanning the whole last page of the paper) we plot various relevant measures obtained with a calibration of our model when driving the open C string of a cello with constant bow velocity $v_b = 0.15$ m/s, constant relative bow-bridge distance $\beta = 0.07$, and a uniformly distributed bow force $F_b = 300$ N/m. A total of 60 equivalent hair-string segments were used to simulate 1 cm of bow width in contact with the string. The configuration was chosen so that it was straightforward to observe temperature diffusion, the histheretic behaviour of friction, partial backward slips, partial forward slips (observable in the top left corner of friction curve corresponding to the nut half of the bow-string contact, and also in the temperature profile), and hair dynamics in both planes. Regarding temperature ranges, note that because the friction dependence with temperature is an arbitrary function (see Section 3), different parameter choices can be made valid, allowing for certain flexibility. For clarity, in Figure 7 we additionally display the spatio-temporal distribution of friction force F_s^x (top) and hair relative horizontal velocity v_h^x (bottom) as seen from the nut side of the bow-string contact, positively showing the differences between the oscillations suffered by the hair during sticking and slipping. Finally, the effect of choice of damping for the equivalent representation of the hairs in the vertical plane can be observed in Figure 8, where vertical waves arriving as reflected from the bridge get progressively attenuated as they go through the bow-string contact.

6. PRELIMINARY TESTS

Our motivation is to construct a reliable platform that, by providing means for simulating the qualitative nature of bowed strings as observed in previous studies, can serve as a basis for developing sound synthesis. Because we face iterative tests involving calibration both of the physical model and of the bowing synthesizer, an important consideration for our approach is efficiency. We have decided to implement our model entirely in plain C so that time computation can be minimized, always aiming at real-time. For the time being, we have discarded parallel computation of any kind.

Many parameters are involved in the physical modeling framework introduced here. It is not the aim of this paper to provide a study on parameter dependence, but to introduce our model and to report on its current state and qualitative behavior. The preliminary tests we carried out with our system are very promising, both in terms of stability and qualitative nature, and also regarding efficiency. The design parameter that presents a most dramatic effect on computation cost is the spatial discretization Δx, which directly translates into the number of nodes used to model bow-string interaction. For a desired Δx, stability imposes Δt.

7. OUTLOOK

We have reported on the current state of our refinement over current bowed-string simulation approaches. Our model is able to match the qualitative nature of previously observed behaviors, but incorporating innovative aspects such as a finite-width dynamic friction model, or a modified Friedlander construction allowing for an efficient solution of nonlinear string-hair dynamics. The model offers a promising compromise between detail and computational cost. Clear next steps are adding torsional string vibration, and further investigating and implementing the modulation of hair physical constants [20] as a function of varying bow force or bowing position. Moreover, we currently prepare extended
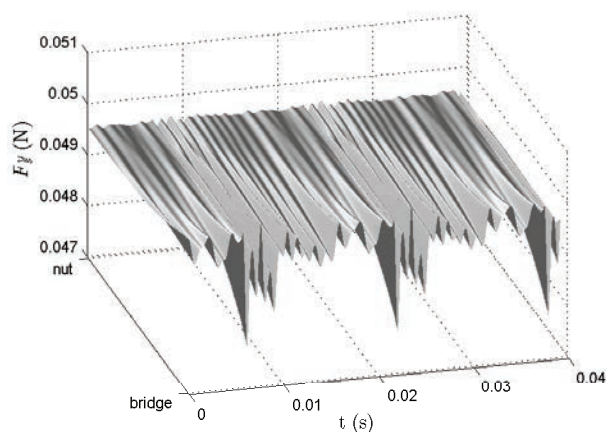
Figure 8: Illustration of the spatio-temporal distribution of the effective bow (vertical) force F_s^y for a simulation with increased hair damping.

tests with synthetic bowing data in order to produce realistic musical sounds which could serve as a basis for evaluating which model features or parameter configurations are perceptually more relevant.

Acknowledgments

8. REFERENCES

[1] E. Maestre, "Modeling instrumental gestures: an analysis/synthesis framework for violin bowing," Ph.D. dissertation, Universitat Pompeu Fabra, 2009.

[2] E. Maestre, M. Blaauw, J. Bonada, E. Guaus, and A. Pérez, "Statistical modeling of bowing control applied to violin sound synthesis," *IEEE Transactions on Audio, Speech, and Language Processing*, vol. 18(4):855–871, 2010.

[3] J. O. Smith, "Physical modeling using digital waveguides," *Computer Music Journal*, vol. 16(4):74–91, 1992.

[4] H. V. Helmholtz, *Lehre von den Tonempfindungen*. Vieweg: Braunschweig, 1862.

[5] C. V. Raman, "On the mechanical theory of vibrations of bowed strings," *Indian Assoc. Cult. Sci. Bull.*, vol. 1-158, 1919.

[6] F. G. Friedlander, "On the oscillations of the bowed string," *Proc. Cambridge Phil. Soc.*, vol. 49, pp. 516–530, 1953.

[7] J. B. Keller, "Bowing of violin strings," *Comm. Pure and Applied Maths*, vol. 6, pp. 283–495, 1953.

[8] M. E. McIntyre and J. Woodhouse, "On the fundamentals of bowed string dynamics," *Acustica*, vol. 43(2):93–108, 1979.

[9] J. O. Smith III, "Efficient simulation of the reed-bore and bow-string mechanisms," in *Proc. 1986 Int. Computer Music Conf., The Hague*. Computer Music Association, searchable at `http://quod.lib.umich.edu/i/icmc/`, 1986, pp. 275–280.

[10] J. O. Smith, "Techniques for digital filter design and system identification with application to the violin," Ph.D. dissertation, Stanford University, 1983.

[11] J. Piteroff and J. Woodhouse, "Mechanics of the contact area between a violin bow and a string, Part II: simulating the bowed string," *Acustica - Acta acustica*, vol. 84, pp. 744–757, 1998.

[12] J. H. Smith and J. Woodhouse, "The tribology of rosin," *J. Mech. Phys. Solids*, vol. 48, pp. 1633–1681, 2000.

[13] J. Woodhouse, "Bowed string simulation using a thermal friction model," *Acustica acta acustica*, vol. 89, pp. 355–368, 2003.

[14] J. Woodhouse and P. M. Galluzzo, "The bowed string as we know it today," *Acustica - Acta Acustica*, vol. 90(4):579–589, 2004.

[15] H. Mansour, J. Woodhouse, and G. Scavone, "Time-domain simulation of the bowed cello string: dual-polarization effect," in *International Congress on Acoustics*, 2013.

[16] S. Serafin, F. Avanzini, and D. Rochesso, "Bowed string simulation using an elasto-plastic friction model," in *Proceedings of the Stockholm Music Acoustics Conference*, 2003.

[17] B. Bank and M. Karjalainen, "Passive admittance matrix modeling for guitar synthesis," in *Proc. of the 13th International Conference on Digital Audio Effects*, 2010.

[18] J. O. Smith, *Physical Audio Signal Processing, December 2008 Edition*. http://ccrma.stanford.edu/~jos/pasp/, accessed 2013, online book.

[19] E. Maestre, G. Scavone, and J. O. Smith, "Digital modeling of bridge driving-point admittances from measurements on violin-family instruments," in *Proceedings of the Stockholm Music Acoustics Conference*, 2013.

[20] C. E. Gough, "Violin bow vibrations," *Journal of the Acoustical Society America*, vol. 131(5), pp. 4152–4163, 2012.
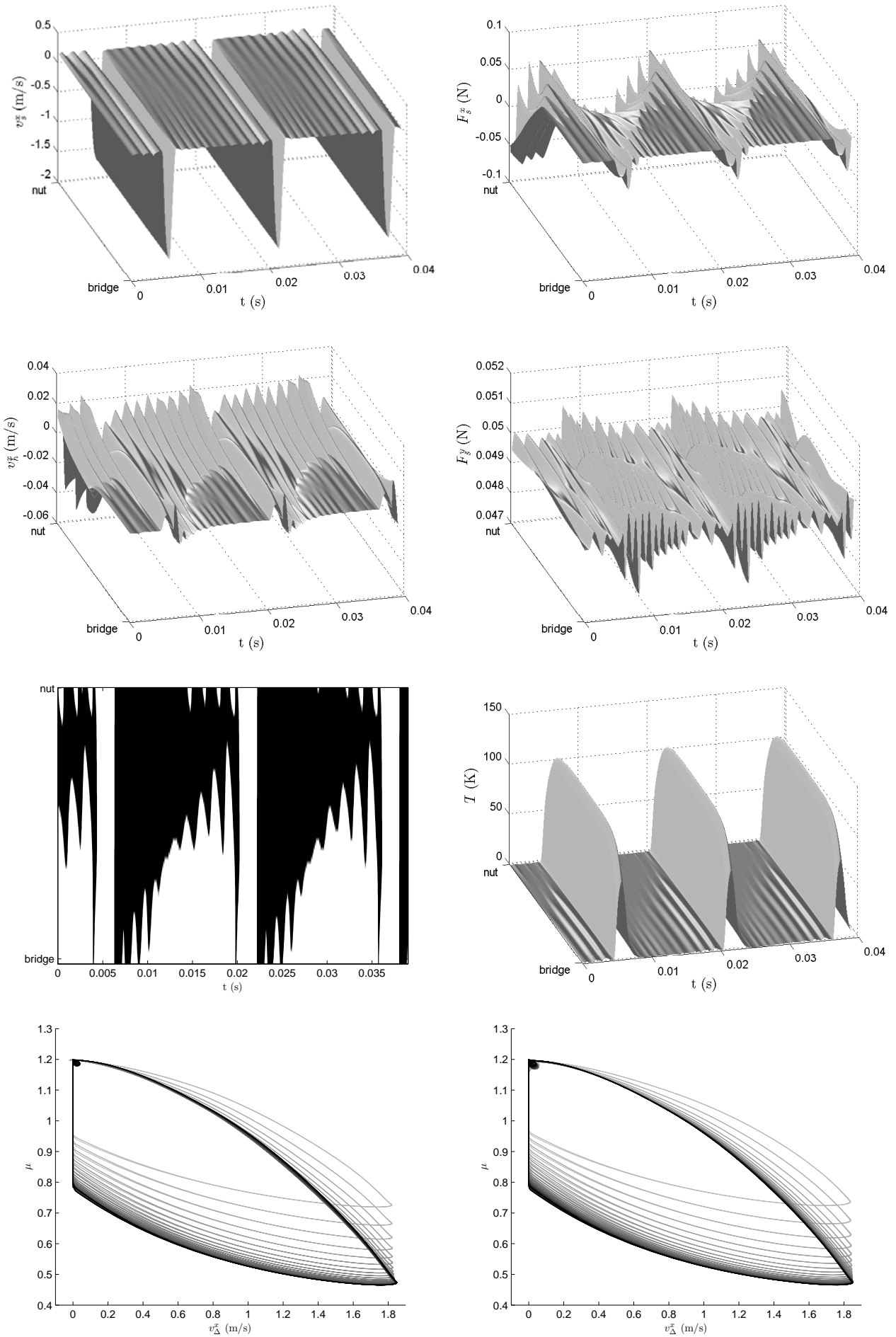
Figure 6: Simulation test, relevant measures. Open C string of a cello driven with $v_b = 0.15$ m/s, $\beta = 0.07$, and $F_b = 300$ N/m. Top to bottom, left to right: String horizontal velocity, friction force, hair relative velocity, effective bow force, friction map (slip: white; stick: black), temperature, sliding velocity vs friction (nut-side half of the bow-string contact; darker greys: towards bow midpoint), sliding velocity vs friction (nut-side half of the bow-string contact; darker greys: towards bow midpoint).